This is a postprint, which has been submitted for peer-review to Quaternary Geochronology and has been published in its final version as Zinelabedin et al., 2022. Testing the potential of using coarse-grain feldspars for post-IRIRSL dating of calcium sulphate-wedge growth in the Atacama Desert. Quaternary Geochronology 71, 101341.

This is a postprint. The article has been submitted for peer-review to Quaternary Geochronology and has been published in its final version as:

Zinelabedin, A., Riedesel, S., Reimann, T., Ritter, B., Dunai, T.J., 2022. Testing the potential of using coarse-grain feldspars for post-IR IRSL dating of calcium sulphate-wedge growth in the Atacama Desert. Quaternary Geochronology 71, 101341.

The article can be accessed by using its DOI:
https://doi.org/10.1016/j.quageo.2022.101341

Testing the potential of using coarse-grain feldspars for post-IR IRSL dating of calcium sulphate-wedge growth in the Atacama Desert

Aline Zinelabedin[1*], Svenja Riedesel[2], Tony Reimann[2], Benedikt Ritter[1], Tibor J. Dunai[1]

[1] Institute of Geology and Mineralogy, University of Cologne, Zülpicher Str. 49b, 50674 Cologne, Germany, *Corresponding author: aline.zinelabedin@uni-koeln.de

[2] Institute of Geography, University of Cologne, Zülpicher Str. 45, 50674 Cologne, Germany

This is a postprint, which has been submitted for peer-review to Quaternary Geochronology and has been published in its final version as Zinelabedin et al., 2022. Testing the potential of using coarse-grain feldspars for post-IRIRSL dating of calcium sulphate-wedge growth in the Atacama Desert. Quaternary Geochronology 71, 101341.

Testing the potential of using coarse-grain feldspars for post-IR IRSL dating of calcium sulphate-wedge growth in the Atacama Desert

Aline Zinelabedin[1*], Svenja Riedesel[2], Tony Reimann[2], Benedikt Ritter[1], Tibor J. Dunai[1]

[1] Institute of Geology and Mineralogy, University of Cologne, Zülpicher Str. 49b, 50674 Cologne, Germany, *Corresponding author: aline.zinelabedin@uni-koeln.de

[2] Institute of Geography, University of Cologne, Zülpicher Str. 45, 50674 Cologne, Germany

Keywords:

Calcium-sulphate wedge, Atacama Desert, feldspar, post-IR IRSL, wedge-growth dating

Abstract

The growth of vertically laminated calcium-sulphate wedges in the Atacama Desert is assumed to be driven by the interaction of moisture supply and salt dynamics in the subsurface. Geochronological data of these wedge laminations is yet sparse but indispensable to resolve wedge-growth phases and episodes of moisture supply and to use these deposits as a palaeoclimate archive in the hyperarid environment. Our pilot study presents a first approach of dating a calcium-sulphate wedge from the Atacama Desert using coarse-grain feldspar luminescence dating. Our results show a widespread and clustered equivalent-dose distribution of two wedge samples from ~20 Gy up to saturation. Optically stimulated luminescence (OSL) of quartz revealed unsuitable properties for dating wedge deposits. Consequently, we applied post-infrared infrared stimulated luminescence (post-IR IRSL) to coarse-grained feldspars. Since feldspar single-grain measurements yielded a low number of luminescent grains, we used 1 mm aliquots as reliable single-grain proxies for genuine single-grain measurements. Data from energy-dispersive x-ray spectroscopy (EDX) showed that the feldspar single grains have large differences in their internal K content, resulting in an averaged internal K content of 3.9 ± 1.0 % for all luminescent grains. This result was subsequently used for dose rate and age calculations. Our results of equivalent-dose distributions and palaeodoses derived from the minimum age model reveal most recent wedge-growth activities at 10.6 ± 2.2 ka and 7.9 ± 1.8 ka for the two wedge samples.

1. Introduction

The presence of subsurface-wedge structures has been confirmed in different parts of the Atacama Desert (e.g. Rech et al., 2003; Buck et al., 2006; Howell, 2009; Rech et al. 2019, Sager et al. 2021), however, questions regarding their formation processes and timing under arid to hyperarid conditions remain unanswered. Yet, chronological data of these wedge structures is sparse, mainly related to the lack of a reliable dating method. Luminescence dating has the potential to determine the timing of wedge formation and has already been applied to quartz and feldspar from other continental deposits in the Atacama Desert (e.g. Ritter et al., 2019; del Río et al., 2019; Medialdea et al., 2020, Bartz et al., 2020a, b). Here we test its application to date calcium-sulphate wedges in the Atacama Desert.

Calcium-sulphate wedges are assumed to be formed similarly to sand and ice wedges in periglacial environments (Howell, 2009); in lieu of the freezing and thawing cycles, it is the (re-) crystallization and phase transitions of calcium-sulphate phases of gypsic soils that create the subsurface stress regime and ensuring clast movement. De-hydration of calcium-sulphate phases is invariably accompanied with as decrease in volume, creating space for soil crack formation. The initial cracks are filled with aeolian and/or fluvial detrital sediments, initially cemented with fully hydrated calcium sulphate (i.e. gypsum, $CaSO_4 \cdot 2H_2O$). On dehydration (to bassanite $CaSO_4 \cdot ½H_2O$, or anhydrite $CaSO_4$) the crack may re-open, for a following filling and opening cycle (e.g. Cook and Warren, 1973; Buck et al., 2006; Howell et al., 2006; Howell, 2009). After multiple cycles, these subsurface processes form a sequence of fine vertical laminations, often symmetrical to the soil crack (Howell, 2009).

A unique subsurface-wedge network is outcropped on an alluvial fan in the northern Atacama Desert (Fig. 1A). The study site (19° 39’ 34.02’’ S, 69° 35’ 51.4’’ W, 1627 m a.s.l.) is a ~ 30 m long trench in the central part of the Aroma fan within the Pampa del Tamarugal in the northern Central Depression (Tarapacá region). The Aroma fan is enclosed by the Andean Precordillera in the east, and the Coastal Cordillera in the west. The outcrop investigated is characterised by desert pavement on a ~20 cm thick calcium-sulphate crust covering alluvial fan deposits hosting a network of subsurface wedges in ~2 m deep soil cracks. The vertically laminated wedge filling is composed of alluvial fan deposits including clastic material and calcium-sulphate phases. The study site is dominated by hyperarid climate (precipitation of <2 mm/a, Houston et al., 2006). Hyperaridity in the Atacama Desert is assumed to be persistent since the Oligocene to Miocene (Dunai et al., 2005; Evenstar et al., 2009, Ritter et al., 2018). In contrast, younger Late Pliocene onsets are proposed by Hartley and Chong (2002) and Amundson et al. (2012) for areas in the Precordillera.

Geochronological data of this calcium-sulphate wedge lamination (Fig. 1D, E) is indispensable to use these geomorphological features as a terrestrial proxy record of paleoclimate at the fringe of the dry-core of the Atacama Desert. Wedge structures in periglacial environments have also been used successfully as palaeoclimate and palaeoenvironment archives (e. g. Williams, 1986; Opel et al., 2018; Campbell et al., 2021), where geochronological data of wedge-sediment fillings were used to gain information on the timing of cryoturbation processes and wedge growth. Luminescence dating has been applied on fillings of relict sand wedges and composite-wedge pseudomorphs to obtain absolute ages and palaeoclimatic information of these periglacial geomorphological features (e.g. Porter et al., 2001; Bateman et al., 2008; Buylaert et al., 2009a; Schaetzl, et al., 2021).

However, Luminescence dating of calcium-sulphate wedge lamination has not yet been applied to constrain the timing of calcium-sulphate wedge growth in hyperarid environments. This study aims at testing the potential of luminescence dating of quartz and feldspar on subsamples of calcium-sulphate wedges from the Aroma fan, to verify the hypothesis that these subsurface structures can be used as terrestrial palaeoclimate archives in the hyperarid Atacama Desert.

This is a postprint, which has been submitted for peer-review to Quaternary Geochronology and has been published in its final version as Zinelabedin et al., 2022. Testing the potential of using coarse-grain feldspars for post-IRIRSL dating of calcium sulphate-wedge growth in the Atacama Desert. Quaternary Geochronology 71, 101341.

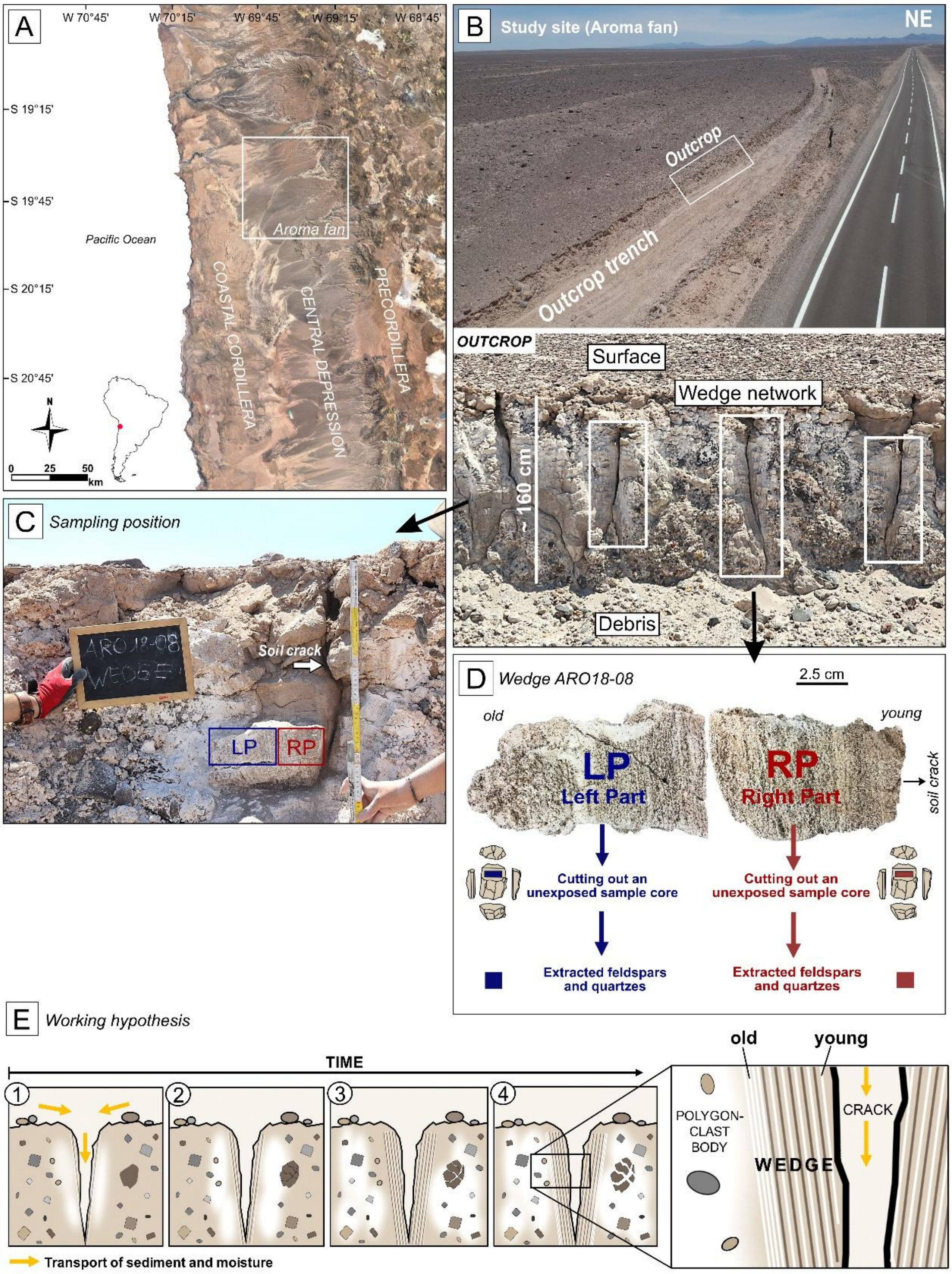

Fig. 1. A) Overview of the study area. The map shows the position of the Aroma fan within the Central Depression in the Atacama Desert (based on Google Earth image: ©2021 Image Landsat/Copernicus - Data SIO, NOAA, U.S. Navy, NGA, GEBCO). B) The drone photograph of the study site shows the outcrop trench, the site surface and an outcrop close-up below showing the subsurface-wedge network outcroped in the trench. C) Close-up of the sampling position of the analysed wedge from approximately 45 cm depth. D) Photograph and sampling strategy of the wedge sample. There are cut out two unexposed sample cores from the right and left part of the wedge under red-light conditions to extract coarse-grain quartzes and feldspars. E) Working hypothesis of the wedge formation. The formation of the vertical wedge lamination is due to the transport and deposition of sediment into the subsurface crack formed due to subsurface pressure induced by salt dynamics. The interaction between salt dynamics and

sediment transport lead to multiple re-openings and re-fillings of the cracks over time. Consequently, the deposits or laminae near the crack are assumed to be younger than those near the polygon-clast body.

2. Material and Methods

2.1 Sample preparation

Subsampling and sample preparation were conducted under subdued red-light conditions in the Cologne Luminescence Laboratory (CLL) of the Institute of Geography of the University of Cologne. Prior to the sample preparation, samples ARO18-08-LP and ARO18-08-RP were extracted by sawing off outer parts of wedge material using a Bühler Abrasimet 250 saw to obtain an unexposed sample of each wedge part (cf. Fig. 1D). Subsequently, these samples were washed with hydrochloric acid (HCl; 10%) to remove calcium sulphate and carbonates. The samples were treated with hydrogen peroxide (H_2O_2; 10%) to remove organic material and sodium oxalate ($Na_2C_2O_4$; 0.01 N) was used to disperse the sediment particles. Subsequently, the samples were dry sieved to extract the 200–250 µm fraction, which was density separated using sodium polytungstate to separate quartz (2.68 g/cm^3 > ρ > 2.62 g/cm^3) and feldspar fractions (ρ < 2.58 g/cm^3). The quartz fraction was etched with concentrated hydrofluoric acid (HF; 40%) for 40 min and subsequently rinsed with HCl (10%) to remove any fluorides. After etching the quartz fraction was re-sieved.

For luminescence measurements, multiple-grain quartz and feldspar aliquots were fixed with silicone spray on stainless steel discs. The size of the aliquot patches was 2 mm and 4 mm for the pre-tests of quartz and feldspar, respectively, and 1 mm for the equivalent-dose measurements of the feldspar-rich extracts. For feldspar single-grain measurements, the grains were brushed into 300 µm holes of single-grain discs.

2.2 Measurement of quartz samples

The suitability of quartz coarse-grain material for optically stimulated luminescence (OSL) dating was tested on multiple-grain aliquots (2 mm diameter) by applying the single-aliquot regenerative dose protocol (SAR; Murray & Wintle, 2000). A preheat temperature of 220 °C (10 s, 5 °C/s) and a test dose cutheat temperature of 200°C were used. The OSL signal was measured at 125 °C for 40 s. The measurements were performed on a Risø TL/OSL DA20 reader equipped with a ^{90}Sr/^{90}Y source delivering ~0.1 Gy/s at the sample position. The quartz OSL signal was stimulated using blue LEDs (470 nm, 80mW/cm^2, measurements done at 90 % power) and was collected through a 7.5 mm thick Schott U340 filter. Initial tests on quartz showed low luminescence-signal intensities and a signal dominated by a slow component (cf. Fig. S1 in the supplementary material). Quartz is therefore not considered further in this study.

2.3 Measurement of feldspar samples

Multiple-grain feldspar aliquot measurements, including pre-test and equivalent dose measurements, were performed on a Risø TL/OSL DA20 reader equipped with a $^{90}Sr/^{90}Y$ beta source delivering a dose rate of ~0.07 Gy/s at the sample position. Single-grain measurements were performed on a Risø TL/OSL DA20 reader equipped with a $^{90}Sr/^{90}Y$ beta source delivering a dose rate of ~ 0.1 Gy/s. The multi-grain aliquots were measured using IR-LEDs (850 nm, FWHM 40 nm, 300 mW/cm^2, measurements performed using 90% power,) and detected through a 3 mm thick Chroma D410/30x LOT interference filter. Feldspar single-grains were stimulated using an IR-laser (830 nm, 150 mW) and the signal was detected using a filter combination of a 2 mm Schott BG-39 and a 3 mm Corning 7-59.

The SAR protocol (Murray & Wintle, 2000) adapted to feldspars (Wallinga et al., 2000) was used by applying the post-infrared infrared stimulated luminescence (post-IR IRSL) procedure (Thomsen et al., 2008; Buylaert et al., 2009b) (cf. Table. 1).

To enable an informed decision on the most suitable preheat and stimulation temperature combination for dating, six different preheat and post-IR IRSL measurement temperatures were tested using a dose-recovery preheat plateau test (DRT-PHPT) and a residual preheat plateau test (R-PHPT) on sample ARO-18-08-LP. The DR-PHPT was performed using a given dose of 150 Gy. Three 4 mm aliquots were measured per temperature combination. Preheat temperatures ranged from 190 °C to 320 °C. The post-IR IRSL signal was measured at temperatures 25-30 °C below the preheat temperature. The first IRSL stimulation temperature was kept at 50 °C. Prior to the DRT-PHPT and R-PHPT the aliquots were bleached for 24 h in a Hönle SOL2 solar simulator. Aliquots measured were accepted when their signals and dose-response curves passed the rejection criteria, which included a recycling ratio within 10 % of unity, a maximum test dose error of 10 %, and a T_n signal with intensities of more than 3 σ above background. Dose-recovery ratios were calculated after subtraction of residuals remaining after 24 h of SOL2 bleaching. A dose-recovery ratio within 10 % of unity was regarded acceptable for further consideration of the chosen temperature.

Potential variations in fading rate with preheat and stimulation temperature were investigated using a fading preheat plateau test (F-PHPT) on four different temperature combinations using 4 mm aliquots of sample ARO-18-08-LP. Also, here three aliquots were measured per temperature combination investigated. Fading measurements were conducted after Auclair et al. (2003).

Table 1: SAR procedure for coarse-grain feldspar aliquots and single-grain measurements. For single-grain measurements the stimulation times were adapted. For $IRSL_{50}$ each grain was stimulated for 2 s, and for post-IR $IRSL_{225}$ measurements each grain was stimulated for 3 s (instrumental details of the single-grain set-up are provided in Reimann et al. 2012).

Step	Treatment	Obtained
1	Beta irradiation	
2	Preheat at 250 °C (2 °C/s) for 60 s	
3	$IRSL_{50}$ for 200 s	L_x
4	Post-IR $IRSL_{225}$ for 300 s	L_x
5	Test dose	
6	Preheat at 250 °C (2 °C/s) for 60 s	
7	$IRSL_{50}$ for 200 s	T_x
8	Post-IR $IRSL_{225}$ for 300 s	T_x

2.4 Dosimetry

The content of uranium (U), thorium (Th), and potassium (K) were measured using high-resolution gamma spectrometry (Ortec Profile MiSeries GEM Coaxial P-type high-precision Germanium Gamma-Ray detector) at the CLL (Table 2). Prior to the measurement, 183 g of dried and homogenised material of ARO18-08-RP and 191 g material from ARO18-08-LP was stored in an airtight container for four weeks to compensate for potential radon loss induced by sample preparation. The activities of isotopes of U- and Th-decay series were checked for potential disequilibrium in the decay chains and no disequilibrium was found. The internal K content was determined for the analysed single-grain discs of the feldspar samples to check a correlation between mineralogical compositions of the individual feldspar grains and their luminescence signal. For internal K content determination energy-dispersive x-ray spectroscopy (EDX) was used. The EDX is attached to a Zeiss Sigma 300-VP scanning electron microscope (SEM)). The dose-rate calculations (Table 2) were performed using the DRAC Calculator v1.2 (Durcan et al., 2015). Dose-rate conversion factors from Guèrin et al. (2011), alpha-grain size attenuation coefficients from Brennan et al., (1991), beta-grain size attenuation coefficients from Guèrin et al. (2012) and an alpha efficiency provided by Kreutzer et al. (2014) for the post-IR $IRSL_{225}$ signal were used. The contribution of the cosmic dose rate was estimated following Prescott and Hutton (1994).

A water content of 2 ± 1 % was calculated for ARO18-08-LP and ARO18-08-RP relative to the dried sample weight. The low water content of the wedge samples approximates low water contents of samples from the Atacama Desert (5 ± 2 %, Nash et al., 2018) and from central Chile (0–6 %, Preusser et al., 2003).

The assessed density of the wedge samples ARO18-08-LP and ARO18-08-RP is based on a photogrammetric image of a wedge created with Agisoft Metashape Professional Software version 1.7.0. The wedge used for photogrammetry originates from the same outcrop (Aroma fan) as the wedge samples ARO18-08-LP and ARO18-08-RP used for luminescence dating. Prior to volume and density calculations, the wedge was weighted (278.74 ± 0.01 g). The calculated volume of the wedge is 155.89 ± 1.56 cm^3 and the calculated density is 1.79 ± 0.02 g/cm^3.

2.5 Chemical composition of feldspar grains

The chemical composition of feldspar single grains was determined using an EDX-attachment of a Zeiss Sigma 300-VP scanning electron microscope. The compositions of the individual feldspars were calculated to determine the molecular formula of the feldspar based on eight oxygen by stoichiometry. Three oxides, K_2O, CaO, and Na_2O, were used for the calculations of the triangular plot coordinates of the ternary feldspar diagrams. The oxides K_2O, CaO, Na_2O, Fe_2O_3, Al_2O_3, TiO_2, and MgO were used to create boxplots to check the oxide distribution in luminescent and non-luminescent feldspar grains from ARO18-08-LP and ARO18-08-RP (cf. Fig. S2 and S3 in the supplementary material).

3. Results

3.1 Protocol selection

Figure 2 shows the results of the pre-tests applied to feldspar aliquots of ARO18-08-LP using a post-IR IRSL protocol (Table 1; Thomson et al., 2008; Buylaert et al., 2009b). The data points of the pre-tests (Fig. 2A–C) represent the average of three 4 mm aliquots each and their respective standard deviation for $IRSL_{50}$ (measured as part of the post-IR IRSL protocol) and post-IR IRSL (T 25/30 °C < Preheat T) signals. The selection of the chosen preheat temperature includes the results of the DRT-PHP in combination with the measured R-PHPT and the F-PHPT. A post-IR_{50} $IRSL_{225}$ protocol using a 60 s preheat at 250 °C was chosen for all further measurements (Table 1), as this temperature combination passed the dose-recovery test for both IRSL signals investigated, showed relatively low residuals and negligible fading for the post-IR IRSL signal. (Fig. 2A–C; highlighted in grey). The chosen temperature combination was then also validated for sample ARO-18-08-RP using dose-recovery tests. To account for any wide-spread equivalent dose values, additional dose-recovery tests were performed on both samples using irradiation doses of 20 and 60 Gy. Figure 2D shows that the dose-recovery test of the post-IR $IRSL_{225}$ protocol for given doses of 20, 60, and 150 Gy is within the deviations of 10 % for both ARO18-08-LP and ARO18-08-RP.

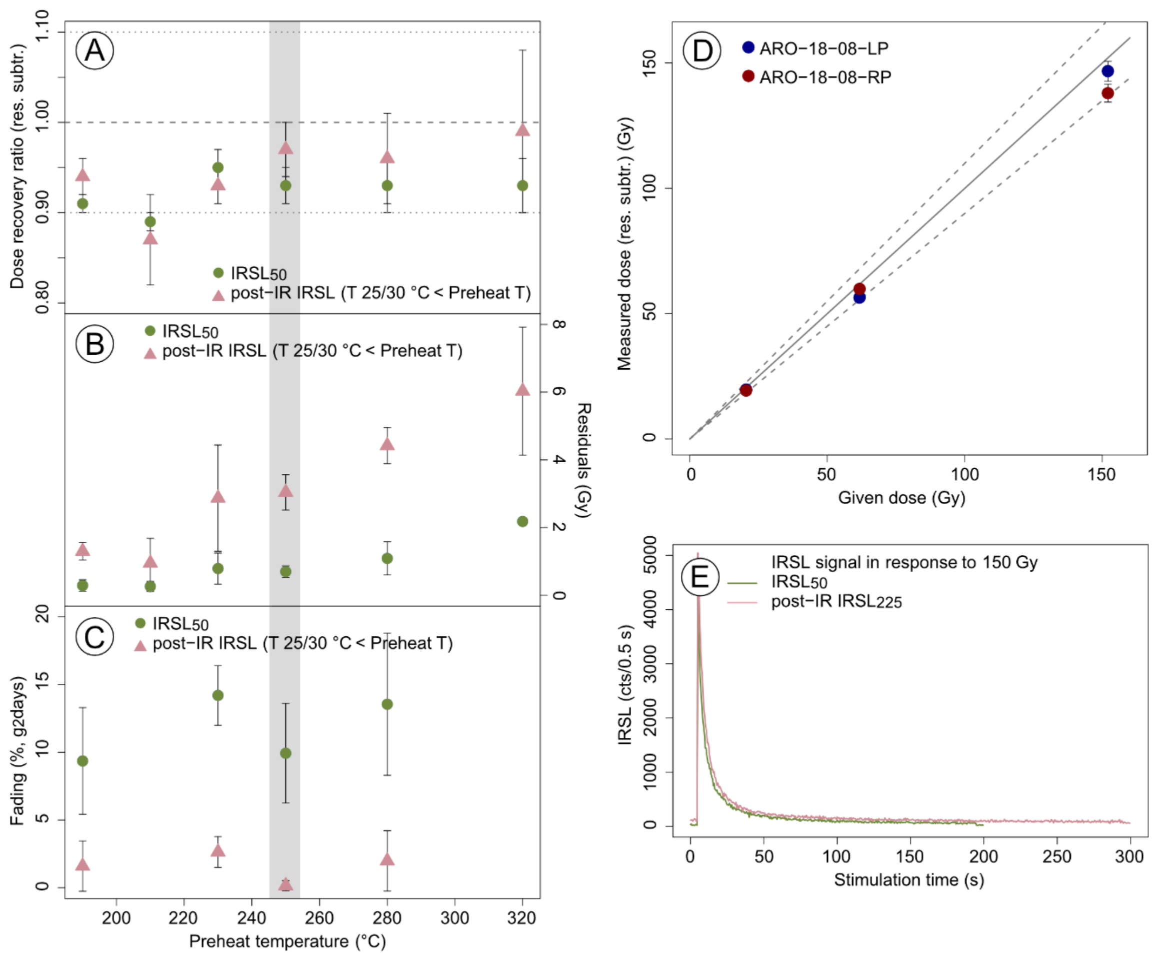

Fig. 2. A) Results of a dose-recovery test (150 Gy) after subtraction of residuals for different preheat and post-IR IRSL temperature combinations, B) residuals measured after 24 h hours of solar simulator bleaching, and C) results of a laboratory fading test performed on sample ARO-18-08-LP. The data points represent the average of three aliquots (4 mm diameter aliquots) and the standard deviation of these measurements. The chosen temperature combination resulting in the post-IR $IRSL_{225}$ protocol is shaded in grey. D) Dose-recovery test for given doses of 20 Gy, 60 Gy and 150 Gy for samples ARO-18-08-LP and ARO-18-08-RP for the chosen post-IR $IRSL_{225}$ protocol. Three 4 mm aliquots were measured per sample and the residuals were subtracted from the measured dose. E) IRSL decay curves for the $IRSL_{50}$ and post-IR $IRSL_{225}$ signals measured within a post-IR $IRSL_{225}$ protocol in response to a laboratory dose of 150 Gy. The curves shown here are from a 4 mm aliquot of sample ARO-18-08-LP.

This is a postprint, which has been submitted for peer-review to Quaternary Geochronology and has been published in its final version as Zinelabedin et al., 2022. Testing the potential of using coarse-grain feldspars for post-IRIRSL dating of calcium sulphate-wedge growth in the Atacama Desert. Quaternary Geochronology 71, 101341.

3.2 Single-grain results of feldspars

The single-grain results of samples ARO18-08-LP and ARO18-08-RP show a small number of luminescent feldspar grains (T_n more than three sigma above background) per single-grain disc (number of luminescent grains: ~1/100 grains). Even a smaller number of grains passed the rejection criteria (recycling ratio within 10 % of unity and a maximum test dose error (10 %)). In order to check a correlation between mineralogical composition and the luminescence signal of feldspar single grains, an EDX analysis was performed. Figure 3 shows two feldspar ternary diagrams of ARO18-08-LP (Fig. 3A) and ARO18-08-RP (Fig. 3B) with the mineralogical compositions of luminescent (red circles) and non-luminescent feldspar (grey triangles) grains from the single-grain discs. In general, both samples are characterised by a majority of Ca-Na-rich grains. The luminescent feldspar grains of ARO18-08-LP are dominated by K-rich feldspars, whereas the luminescent feldspar grains from ARO18-08-RP are dominated by Ca-Na-rich grains lying in the field of the miscibility gap of feldspars Additionally, the low average K content (3.9 ± 1.0 %) measured for the individual luminescent grains will also help in adjusting the internal K content for dose-rate calculations (Fig. S2 and S3).

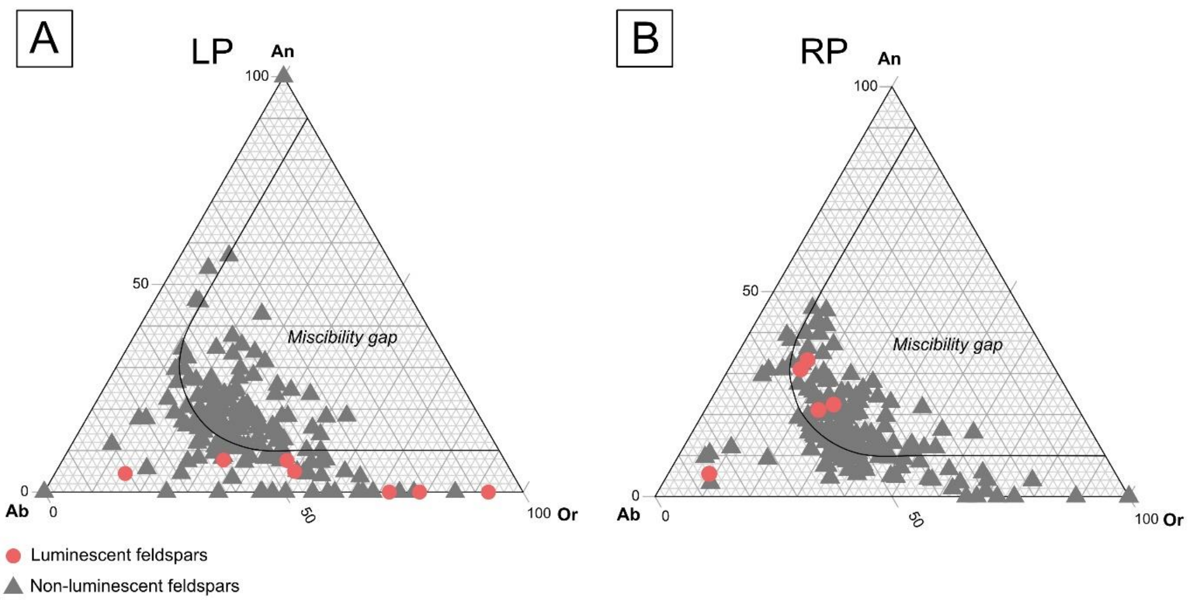

Fig. 2) Feldspar ternary diagrams of ARO18-08-LP and ARO18-08-RP showing the compositions of feldspars from single-grain measurements. Red cycles indicate luminescent and grey triangles represent non-luminescent feldspar grains. Luminescent grains are characterised showing sufficient test-luminescence responses in the post-IR IRSL$_{225}$ signal (T_n more than 3 sigma above background). The end members are Ab = Albite ($NaAlSi_3O_8$), An = Anorthite ($CaAl_2Si_2O_8$), Or = Orthoclase ($KAlSi_3O_8$). A) Feldspar compositions of ARO18-08-LP. B) Feldspar compositions of ARO18-08-RP.

3.3 Equivalent-dose determination of feldspar aliquots

Due to the low yield of luminescent grains, equivalent-dose (D_e) measurements were performed using 1 mm aliquots as proxy for genuine single-grain measurements of both wedge-part samples ARO18-08-LP and ARO18-08-RP using the post-IR $IRSL_{225}$ protocol (Table 1). Figure 4 shows the equivalent-dose range of accepted aliquots from ARO18-08-LP and ARO18-08-RP as well as the number of saturated aliquots (>2 x D_0; Wintle and Murray, 2006) and aliquots which did not pass the rejection criteria for the post-IR $IRSL_{225}$ signal. Due to the high fading rates (g_{2days}: >9 %/decade, cf. Table 2) of the $IRSL_{50}$ signal, measured as part of the post-IR_{50} $IRSL_{225}$ protocol, equivalent doses obtained for this signal are not considered for age calculations, but a minimum palaeodose was calculated for both samples and is given in Table 2. The post-IR $IRSL_{225}$ results of both samples show a wide range of D_e values spanning from ~20 Gy up to saturation. In order to obtain preliminary information on the palaeodose of the samples, and thus on the most recent wedge activity phase, the logged three-parameter minimum age model (MAM) was applied using the calc_MinDose() function in R (Galbraith et al. 1999, R Core Team, 2021; Burrow, et al., 2021).

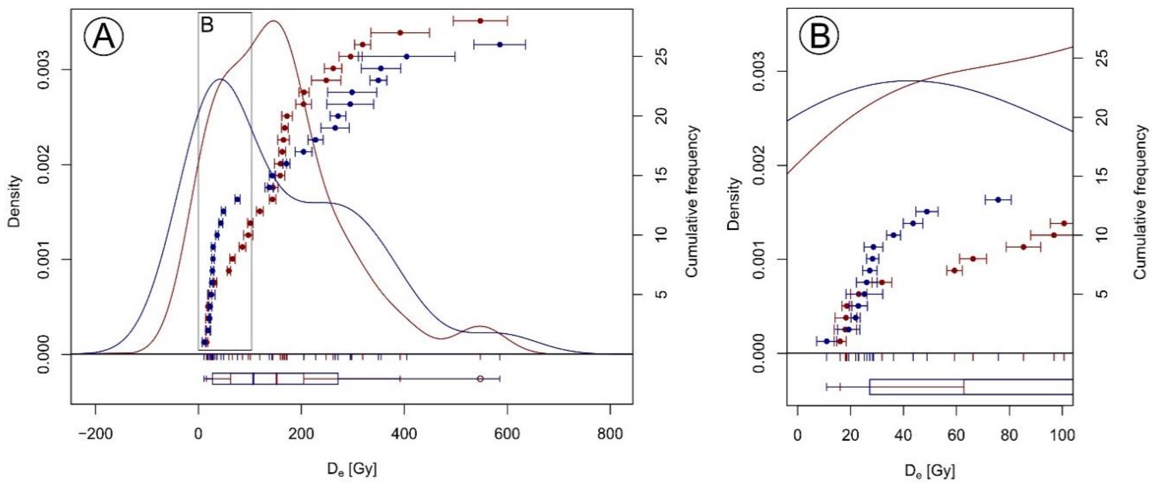

Fig. 4. Post-IR $IRSL_{225}$ equivalent doses from 1 mm aliquots of two samples ARO18-08-LP (blue) and ARO18-08-RP (red). ARO18-08-LP: Total number of measured discs = 62, accepted = 26, saturated = 7, do not passed rejection criteria = 29. ARO18-08-RP: Total number of measured discs = 56, accepted = 28, saturated = 4, do not passed the rejection criteria = 24. A) Equivalent-dose distribution of 1 mm feldspar aliquots from ARO18-08-LP (blue circles) and ARO18-08-RP (red circles). B) Close-up of the data set with the lowest D_e values being significant for MAM calculations.

This is a postprint, which has been submitted for peer-review to Quaternary Geochronology and has been published in its final version as Zinelabedin et al., 2022. Testing the potential of using coarse-grain feldspars for post-IRIRSL dating of calcium sulphate-wedge growth in the Atacama Desert. Quaternary Geochronology 71, 101341.

Table. 2: U, Th, and K content determined by high-resolution gamma spectrometry, the measured water content, and the internal K content (average and standard error) of luminescent single grains derived from SEM measurements. The dose rates were calculated using DRAC (Durcan et al., 2015). [1]dose for fading 150 Gy [2]IRSL$_{50}$ D$_e$ distribution of ARO18-08-LP and -RP are shown in Figure S4 in the supplementary material

Sample ID	Depth [m]	U [ppm]	Th [ppm]	K [%]	Water content [%]	Internal K [%]	Cosmic dose rate [Gy/ka]	External dose rate [Gy/ka]	Internal dose rate [Gy/ka]	Environmental dose rate [Gy/ka]	MAM palaeodose [Gy][2]	Fading (%, g2days)[1]	Age (ka)
ARO18-08-LP (IRSL$_{50}$)	0.45 ± 0.03	1.43 ± 0.09	4.02 ± 0.26	1.23 ± 0.02	2.0 ± 1.0	3.9 ± 1.0	0.25 ± 0.03	2.09 ± 0.04	0.25 ± 0.07	2.34 ± 0.08	5.36 ± 1.32	9.93 ± 3.68	
ARO18-08-LP (post-IR IRSL$_{225}$)	0.45 ± 0.03	1.43 ± 0.09	4.02 ± 0.26	1.23 ± 0.02	2.0 ± 1.0	3.9 ± 1.0	0.25 ± 0.03	2.12 ± 0.04	0.25 ± 0.07	2.37 ± 0.08	25.31 ± 5.08	0.15 ± 0.37	10.6 ± 2.2
ARO18-08-RP (IRSL$_{50}$)	0.45 ± 0.03	1.43 ± 0.09	4.02 ± 0.26	1.23 ± 0.02	2.0 ± 1.0	3.9 ± 1.0	0.25 ± 0.03	2.34 ± 0.04	0.25 ± 0.07	2.60 ± 0.08	8.26 ± 2.33	10.53 ± 3.43	
ARO18-08-RP (post-IR IRSL$_{225}$)	0.45 ± 0.03	1.44 ± 0.09	5.15 ± 0.32	1.41 ± 0.02	2.0 ± 1.0	3.9 ± 1.0	0.25 ± 0.03	2.38 ± 0.05	0.25 ± 0.07	2.64 ± 0.09	20.92 ± 4.71	0.06 ± 0.32	7.9 ± 1.8

4. Discussion

4.1 Luminescence characteristics

In order to resolve wedge-growth activity in the hyperarid Atacama Desert in northern Chile, we tested the application of quartz OSL and feldspar post-IR IRSL dating to clastic sediments trapped in calcium-sulphate wedges of the Aroma fan in the Atacama Desert.

In agreement with previous luminescence-dating studies on Atacama sediments (e.g. Nash et al., 2018; del Río et al., 2019; Medialdea et al., 2020) the luminescence properties of quartz were found to be inappropriate for luminescence dating due to low signal intensities and a dominant slow component (cf. Fig. S1).

However, first tests on sand-sized feldspar grains show promising luminescence behaviour and indicate the potential of using feldspars to constrain calcium-sulphate wedge-growth activity in this hyperarid environment (cf. Fig. 2). Nevertheless, low numbers of individual luminescent grains prevented us from using single-grain luminescence dating of coarse-grain feldspars to constrain wedge formations. Previously, del Río et al. (2019), Ritter et al. (2019), Bartz et al. (2020a, b), and Medialdea et al. (2020) successfully used feldspar-luminescence dating to constrain the depositional history of various sedimentary sequences within the Atacama Desert. Veit et al. (2015) applied feldspar-luminescence dating to aeolian sand dunes and dunes with intercalated palaeosols to constrain palaeowind regimes in semi-arid Chile. These studies also used the post-IR $IRSL_{225}$ protocol and are therefore comparable with the present study. Whilst Veit et al. (2015), del Río et al. (2019), and Bartz et al. (2020a, b) performed their feldspar-luminescence measurements on coarse-grain aliquots, the results of Ritter et al. (2019) are based on polymineral fine grains, and Bartz et al. (2020a) and Medialdea et al. (2020) also presented feldspar single-grain results. Bartz et al., 2020a showed single-grain results for one of their samples. This sample resulted in ~57 % and ~30 % luminescent grains for the investigated $IRSL_{50}$ and post-IR $IRSL_{225}$ signals, respectively. In contrast, Medialdea et al. (2020) showed lower percentages of accepted grains in relation to the total number of grains, resulting in only ~10 to ~20 % of grains accepted for age calculations. The single-grain results presented in the current study yield even lower numbers of luminescent grains in general (~1 grain/100 grains measured on average). Unfortunately, the number of single-grain discs measured (n = 4 for each sample) is too low to create synthetic aliquot data (e.g. Stone et al., 2012) meaningful enough in relation to the wide-spread in equivalent doses observed using 1 mm aliquots (cf. Fig. 4). Due to the low total number of luminescent grains, and the number of aliquots, which did not result in an equivalent dose (cf. Fig. 4), we estimate potential averaging effects (Duller, 2008; Reimann et al., 2012) in the measurements of small aliquots in comparison to true single-grain measurements to be relatively low. Thus, we consider our 1 mm aliquot measurements as reliable single-grain proxies.

To investigate the source of the low yield of luminescent grains, feldspar single grains were chemically characterised using EDX. The chemical composition of luminescent and non-luminescent grains was compared (Figs. 3, S2, S3).

As shown in the feldspar ternary diagrams and boxplots (Figs. 3, S2, S3) of ARO18-08-LP and ARO18-08-RP, the luminescent grains of ARO18-08-LP are dominant by K-rich feldspars, while the luminescent grains of ARO18-08-RP are dominated by Ca-Na-rich grains lying in the field of the miscibility gap in the feldspar ternary diagram. The statistical distribution of all investigated oxides shown in the boxplots (Figs. S2 and S3) indicate no correlation between chemical composition and the luminescent signal intensities. However, the boxplots of both samples (Figs. S2, S3) show high Fe contents in the feldspar grains, which is higher than it would be expected for feldspars. This could potentially indicate Fe-rich varnish occurring on clasts in hyperarid envirnonments such as in the Atacama Desert (e.g. Kuhlman et al., 2008). Fe-rich coatings could possibly affect the internal K determination or be responsible for the low yield of luminescent grains in the samples. Therefore, the composition of feldspar grains and potential Fe-rich coatings will be examined further in future investigations.

Smedley et al. (2012) compared blue luminescence signal intensities and internal K contents of feldspar single grains and found that the majority of the signals is emitted by feldspar grains with the highest K contents (average K content of these grains: 12.3 %). This observation is in agreement with findings by Huntley and Baril (1997). Smedley et al. (2012) also showed that luminescence arises from grains with K contents below 12 %, but not of grains with K contents below 6 %. The results by Riedesel et al. (2021) on alkali feldspar mineral specimen indicate that the blue luminescence emission is related to interfaces in perthitic feldspar. Since we here observe luminescent and non-luminescent grains of the alkali feldspar and the plagioclase solid solution (Fig. 3), our data set is a valuable addition to the existing research into the source of blue luminescence intensity in chemically different feldspars.

However, these findings complicate future dose-rate calculations using our sample material, as we observe large differences in internal K content for the feldspar grains measured in the present study using EDX and the dominance of Ca-Na-rich grains in ARO18-08-LP and ARO18-08-RP. In agreement with Sontag-González et al. (2021) and O'Gorman et al. (2021), grains with complex mineralogical compositions require the investigation of the mineralogical composition and luminescence properties to assess their suitability for luminescence dating. O'Gorman et al. (2021) analysed the mineralogical composition of composite grains of volcanic origin with regard to luminescence dating on feldspars. The authors found that their luminescent grains have a variety in their averaged internal K content ranging from 0–14 wt%

and tightly clustered distributions of K concentrations with <3 wt%. Smedley et al. (2012) investigated grains with an internal K content of 6–13 % showing IRSL and post-IR IRSL signal and suggested an internal value of 10 ± 2 % for single-grain feldspar dating as a more appropriate approximation than adopting the value of 12 ± 0.5 % (Huntley and Baril, 1997) typically used for multi-grain feldspar-luminescence dating. Since most of our luminescent grains of ARO18-08-LP and ARO18-08-RP show relatively low K contents, published K contents (e.g. Huntley and Baril, 1997; Smedley et al., 2012) would result in an overestimation of internal K concentrations.

Due to large differences in the internal K content between luminescent grains from ARO18-08-LP and ARO18-08-RP and their low proportion, the average (± standard error) internal K content of 3.9 ± 1.0 % for all luminescent grains from both samples is used for dose-rate calculations.

4.2 Equivalent-dose distributions and first chronological indications

The post-IR IRSL equivalent doses of coarse-grain feldspar aliquots from ARO18-08-LP and ARO18-08-RP show a wide range of values from ~20 Gy to saturation. The equivalent-dose distributions are nearly identical for both wedge samples with slight differences at lower equivalent doses (Fig. 4). In general, a clustering of equivalent-dose values is identifiable showing approximately three to four clusters in the full range of D_e results.

Veit et al. (2015) analysed aeolian deposits from central Chile using post-IR $IRSL_{225}$ applied to coarse-grain feldspar aliquots. Due to aeolian sediment transport of the deposits, the authors assume that the sample material is well bleached. Bartz et al. (2020b) used single-grain post-IR $IRSL_{225}$ applied to aeolian, alluvial fan, and marine deposits from the northern Atacama Desert showing a low scatter of D_e values of well-bleached aeolian deposits, and even D_e distributions of samples taken from alluvial fans and marine deposits show less scatter in D_e distributions, compared to the range of D_e values obtained in the present paper (Fig. 4).

The wide range and clustering of post-IR IRSL equivalent doses of the coarse-grain feldspar aliquots from ARO18-08-LP and ARO18-08-RP are thus interpret as likely resulting from wedge-growth activities during multiple active phases of wedge growth and salt dynamics. First calculations of MAM palaeodoses with 25.3 ± 5.1 Gy for ARO18-08-LP and 20.9 ± 4.7 Gy for ARO18-08-RP in relation to environmental dose rates of 2.3 ± 0.1 Gy/ka and 2.6 ± 0.1 Gy/ka, respectively, indicate the most recent wedge-growth activities and salt dynamics at 10.6 ± 2.2 ka for ARO18-08-LP and 7.9 ± 1.8 ka for ARO18-08-RP. However, the nearly identical D_e distribution of both wedge samples indicate a vertical stratigraphy of wedge deposits rather than a horizontal stratigraphy assumed in the wedge-formation hypothesis (cf. Fig. 1E). In order to further precise the investigation of the finely laminated wedge samples and their formation history, we aim to apply spatially-resolved luminescence (e.g. Greilich et al., 2002; Thomsen et al., 2018; Sellwood et al., 2019) and increase the sampling resolution to determine the age progression within the wedge deposits. Due to the heterogenous and complex outcrop structure in which the wedges are incorporated, in-situ gamma spectrometry is also intended to improve dose-rate measurements in regard to gamma dose-rate heterogeneities in the surrounding of the sample material.

Previous paleoclimate records from numerous geo-archives (e.g. alluvial fan deposits, sediment cores of endorheic basins, or colluvial deposits from hillslopes) resolved several fluctuations in aridity for the past ~100–200 ka (e.g. Ritter et al., 2019; del Río et al., 2019; Medialdea et al., 2020, Bartz et al., 2020a, b). Considering the range of equivalent doses from ~20–600 Gy, our post-IR IRSL data from felspars of calcium-sulphate wedges have potential to contribute to the paleoclimate record in the northern Atacama Desert in the time span from the Late Pleistocene up to the Holocene.

5. Conclusion

The present study provides first results of feldspar post-IR IRSL dating of a calcium-sulphate wedge from the hyperarid Atacama Desert revealing a wide range of clustered D_e values from ~20 Gy up to saturation and a nearly identical D_e distribution in two wedge subsamples. From this pilot study we can draw following conclusions:

Initial tests of OSL measurements on quartz extracted from wedge material showed insufficient properties for dating wedge fillings, however, feldspars proved to be suitable for luminescence-dating purposes. Due to the low yield of luminescent feldspar grains in both wedge samples, 1 mm aliquots were used as reliable proxies for genuine single-grain feldspar measurements of the wedge deposits. As EDX data show, the internal K content from the low proportion of luminescent grains differs significantly between the two wedge samples. Thus, the averaged internal K content of 3.9 ± 1.0 % measured for both samples was used as an essential parameter for dose rate and age calculations.

Equivalent-dose distributions and palaeodoses based on the minimum age model revealing the most recent wedge-growth activities and associated salt dynamics at 10.6 ± 2.2 ka for ARO18-08-LP and 7.9 ± 1.8 ka for ARO18-08-RP. The similar distribution of D_e values of both wedge samples indicate that the stratigraphy of wedge deposits contradicts the wedge-formation hypothesis and yet is not resolvable by the current data. However, feldspar post-IR IRSL dating of the wedge-growth activity has potential to date episodes of enhanced moisture supply and resulting salt dynamics in the Atacama Desert for the last three glacial-interglacial cycles.

6. Acknowledgements

This project is affiliated to the Collaborative Research Centre (CRC) 1211 “Earth – Evolution at the Dry Limit” (Grant-No.: 268236062) funded by the German Research Foundation (Deutsche Forschungsgemeinschaft, DFG). We would like to thank Anja Zander (CLL, University of Cologne) for high-resolution gamma-spectrometry measurements and Dominik Brill (CLL, University of Cologne) for help with the subsample sawing. We would also like to thank Hanna Cieszynski (University of Cologne) for the support with the SEM measurements. We thank Nick Pearce (Aberystwyth University) for the spreadsheet used for stoichiometric calculations and Joel Mohren (University of Cologne) for the density calculations of the wedge sample using photogrammetry. We would like to thank the anonymous reviewer for the constructive feedback, which improved our manuscript.

7. References

Amundson, R., Dietrich, W., Bellugi, D., Ewing, S., Nishiizumi, K., Chong, G., Owen, J., Finkel, R., Heimsath, A., Stewart, B., Caffee, M., 2012. Geomorphologic evidence for the late Pliocene onset of hyperaridity in the Atacama Desert. Geol. Soc. Am. Bull. 124, 1048–1070. https://doi.org/10.1130/B30445.1.

Auclair, M., Lamothe, M., Huot, S., 2003. Measurement of anomalous fading for feldspar IRSL using SAR. Radiat. Meas. 37, 487–492. https://doi.org/10.1016/S1350-4487(03)00018-0.

Bartz, M., Duval, M., Brill, D., Zander, A., King, G.E., Rhein, A., Walk, J., Stauch, G., Lehmkuhl, F., Brückner, H., 2020a. Testing the potential of K-feldspar pIR-IRSL and quartz ESR for dating coastal alluvial fan complexes in arid environments. Quaternary International 556, 124–143. https://doi.org/10.1016/j.quaint.2020.03.037.

Bartz, M., Walk, J., Binnie, S.A., Brill, D., Stauch, G., Lehmkuhl, F., Hoffmeister, D., Brückner, H., 2020b. Late Pleistocene alluvial fan evolution along the coastal Atacama Desert (N Chile). Glob. Planet. Change 190, 103091. https://doi.org/10.1016/j.gloplacha.2019.103091.

Bateman, M.D., 2008. Luminescence dating of periglacial sediments and structures. Boreas 37, 574–588. https://doi.org/10.1111/j.1502-3885.2008.00050.x.

Brennan, B.J., Lyons, R.G., Phillips, S.W., 1991. Attenuation of alpha particle track dose for spherical grains. Int. J. Radiat. Appl. Instrum. Part D. Nucl. Tracks Radiat. Meas. 18, 249–253.

Buck, B.J., Rech, J.A., Howell, M.S., Prellwitz, J., Brock, A.L., 2006. A new formation process for patterned ground, Atacama Desert, Chile. Geol.Soc. Am. Bull. Philadelphia Annual Meeting 2006, Philadelphia.

Burow, C., 2021. calc_MinDose: Apply the (un-)logged minimum age model (MAM) after Galbraith et al. (1999) to a given De distribution. Function version 0.4.4. In: Kreutzer, S., Burow, C., Dietze, M., Fuchs, M.C., Schmidt, C., Fischer, M., Friedrich, J., Mercier, N., Philippe, A., Riedesel, S., Autzen, M., Mittelstrass, D., Gray, H.J. (Ed.) Luminescence: Comprehensive Luminescence Dating Data Analysis. R package version 0.9.15. https://CRAN.R-project.org/package=Luminescence.

Buylaert, J.-P., Ghysels, G., Murray, A.S., Thomsen, K.J., Vandenberghe, D., Corte, F. de, Heyse, I., van den Haute, P., 2009a. Optical dating of relict sand wedges and composite-wedge pseudomorphs in Flanders, Belgium. Boreas 38, 160–175. https://doi.org/10.1111/j.1502-3885.2008.00037.x.

Buylaert, J.P., Murray, A.S., Thomsen, K.J., Jain, M., 2009b. Testing the potential of an elevated temperature IRSL signal from K-feldspar. Radiat. Meas. 44, 560–565. https://doi.org/10.1016/j.radmeas.2009.02.007.

Campbell-Heaton, K., Lacelle, D., Fisher, D., 2021. Ice wedges as winter temperature proxy: Principles, limitations and noise in the δ18O records (an example from high Arctic Canada). Quat. Sci. Rev. 269, 107135. https://doi.org/10.1016/j.quascirev.2021.107135.

Cooke and A. Warren 1973. Geomorphology in Deserts. Geol. Mag. 111, 186–187.

del Río, I., Sawakuchi, A.O., González, G., 2019. Luminescence dating of sediments from central Atacama Desert, northern Chile. Quat. Geochronol. 53, 101002. https://doi.org/10.1016/j.quageo.2019.05.001.

Duller, G.A.T., 2008. Single-grain optical dating of Quaternary sediments: why aliquot size matters in luminescence dating. Boreas 37, 589–612. https://doi.org/10.1111/j.1502-3885.2008.00051.x.

Dunai, T.J., González López, G.A., Juez-Larré, J., 2005. Oligocene–Miocene age of aridity in the Atacama Desert revealed by exposure dating of erosion-sensitive landforms. Tectonophysics 33, 321. https://doi.org/10.1130/G21184.1.

Durcan, J.A., King, G.E., Duller, G.A., 2015. DRAC: Dose Rate and Age Calculator for trapped charge dating. Quat. Geochronol. 28, 54–61. https://doi.org/10.1016/j.quageo.2015.03.012.

This is a postprint, which has been submitted for peer-review to Quaternary Geochronology and has been published in its final version as Zinelabedin et al., 2022. Testing the potential of using coarse-grain feldspars for post-IRIRSL dating of calcium sulphate-wedge growth in the Atacama Desert. Quaternary Geochronology 71, 101341.

Evenstar, L.A., Hartley, A.J., Stuart, F.M., Mather, A.E., Rice, C.M., Chong, G., 2009. Multiphase development of the Atacama Planation Surface recorded by cosmogenic 3He exposure ages: Implications for uplift and Cenozoic climate change in western South America. Geol. 37, 27–30. https://doi.org/10.1130/G25437A.1.

Galbraith, R.F., Roberts, R.G., Laslett, G.M., Yoshida, H., Olley, J.M., 1999. Optical dating of single and multiple grains of quartz from Jinmium rock shelter, northern australia: part i, experimental design and statistical models. Archaeometry 41, 339–364. https://doi.org/10.1111/j.1475-4754.1999.tb00987.x.

Greilich, S., Glasmacher, U.A., Wagner, G.A., 2002. Spatially resolved detection of luminescence: a unique tool for archaeochronometry. Die Naturwissenschaften 89, 371–375.

Guérin, G., Mercier, N. and Adamiec, G, 2011. Dose-rate conversion factors: update. Anc. TL 29, 5–8.

Guerin, G., Mercier, N., Nathan, R., Adamiec, C., Lefrais, Y., 2012. On the use of the infinite matrix assumption and associated concepts: a critical review. Radiat. Meas. 47, 778-785. https://doi.org/10.1016/j.radmeas.2012.04.004.

Hartley, A.J., Chong, G., 2002. Late Pliocene age for the Atacama Desert: Implications for the desertification of western South America. Geology 30, 43. https://doi.org/ 10.1130/0091-7613(2002)030<0043:LPAFTA>2.0.CO;2.

Houston, J., 2006. Variability of precipitation in the Atacama Desert: its causes and hydrological impact. Int. J. Climatol. 26, 2181–2198. https://doi.org/10.1002/joc.1359.

Howell, M.S., 2009. Mineralogy and micromorphology of an Atacama Desert soil, Chile: A model for hyperarid pedogenesis: Master's thesis. UNLV Theses, Dissertations, Professional Papers, and Capstones.

Howell, M.S., Buck, B.J., Rech, J.A., Brock, A.L., Prellwitz, J., 2006. Genesis of the Hyperarid Soils of the Atacama Desert: Analogue for Mars?. 18th World Congress of Soil Science, Philadelphia, Pennsylvania.

Huntley, D.J., Baril, M.R., 1997. The K content of the K-feldspars being measured in optical dating or in thermoluminescence dating. Anc. TL 15, 11–13.

Kreutzer, S., Burow, C., Dietze, M., Fuchs, M.C., Schmidt, C., Fischer, M., Friedrich, J., Mercier, N., Philippe, A., Riedesel, S., Autzen, M., Mittelstrass, D., Gray, H.J. (Ed.), 2021. Luminescence: Comprehensive Luminescence Dating Data Analysis. R package version 0.9.15. https://CRAN.R-project.org/package=Luminescence.

Kreutzer, S., Schmidt, C., DeWitt, R., Fuchs, M., 2014. The a-value of polymineral fine grain samples measured with the post-IR IRSL protocol. Radiat. Meas. 69, 18–29. https://doi.org/10.1016/j.radmeas.2014.04.027.

Kuhlman, K.R., Venkat, P., La Duc, M. T., Kuhlman, G.M., McKay, P., 2008. Evidence of a microbial community associated with rock varnish at Yungay, Atacama Desert, Chile. J. Geophys. Res.113, G04022. https://doi:10.1029/2007JG000677.

Medialdea, A., May, S.M., Brill, D., King, G., Ritter, B., Wennrich, V., Bartz, M., Zander, A., Kuiper, K., Hurtado, S., Hoffmeister, D., Schulte, P., Gröbner, M., Opitz, S., Brückner, H., Bubenzer, O., 2020. Identification of humid periods in the Atacama Desert through hillslope activity established by infrared stimulated luminescence (IRSL) dating. Glob. Planet. Change 185, 103086. https://doi.org/10.1016/j.gloplacha.2019.103086.

Murray, A.S., Wintle, A.G., 2000. Luminescence dating of quartz using an improved single-aliquot regenerative-dose protocol. Radiat. Meas. 32, 57-73. https://doi.org/10.1016/S1350-4487(03)00053-2.

Nash, D.J., Bateman, M.D., Bullard, J.E., Latorre, C., 2018. Late Quaternary coastal evolution and aeolian sedimentation in the tectonically-active southern Atacama Desert, Chile. Palaeogeogr. Palaeoclimatol. Palaeoecol. 490, 546–562. https://doi.org/10.1016/j.palaeo.2017.11.040.

O'Gorman, K., Tanner, D., Sontag-González, M., Li, B., Brink, F., Jones, B.G., Dosseto, A., Jatmiko, Roberts, R.G., Jacobs, Z., 2021. Composite grains from volcanic terranes: Internal dose rates of supposed ‘potassium-rich’ feldspar grains used for optical dating at Liang Bua, Indonesia. Quat. Geochronol. 64, 101182. https://doi.org/10.1016/j.quageo.2021.101182.

Opel, T., Meyer, H., Wetterich, S., Laepple, T., Dereviagin, A., Murton, J., 2018. Ice wedges as archives of winter paleoclimate: A review. Permafrost Periglac. Process. 29, 199–209. https://doi.org/10.1002/ppp.1980.

Porter, S.C., Singhvi, A., Zhisheng, Zhongping, L., 2001. Luminescence age and palaeoenvironmental implications of a late Pleistocene ground wedge on the Northeastern Tibetan Plateau. Permafrost Periglac. Process. 12, 203–210. https://doi.org/ 10.1002/ppp.386.

Prescott, J.R. and Hutton, J.T., 1994. Cosmic ray contributions to dose rates for luminescence and ESR dating: Large depths and long-term time variations. Radiat. Meas. 497–500.

Preusser, F., 2003. IRSL dating K-rich feldspars using the SAR protocol: Comparison with indipendent age control. Anc. TL. 21, 17–23.

R Core Team, 2021. R: A language and environment for statistical computing. R Foundation for Statistical Computing. Vienna. Austria. https://www.R-project.org/.

Rech, J.A., Currie, B.S., Jordan, T.E., Riquelme, R., Lehmann, S.B., Kirk-Lawlor, N.E., Li, S., Gooley, J.T., 2019. Massive middle Miocene gypsic paleosols in the Atacama Desert and the formation of the Central Andean rain-shadow. EPSL. 506, 184–194. https://doi.org/10.1016/j.epsl.2018.10.040.

Rech, J.A., Quade, J., Hart, W.S., 2003. Isotopic evidence for the source of Ca and S in soil gypsum, anhydrite and calcite in the Atacama Desert, Chile. Geochim. Cosmochim. Acta 67, 575–586. https://doi.org/10.1016/S0016-7037(02)01175-4.

Reimann, T., Thomsen, K.J., Jain, M., Murray, A.S., Frechen, M., 2012. Single-grain dating of young sediments using the pIRIR signal from feldspar. Quat. Geochronol. 11, 28–41. https://doi.org/10.1016/j.quageo.2012.04.016.

Riedesel, S., Bell, A., Duller, G., Finch, A.A., Jain, M., King, G.E., Pearce, N.J., Roberts, H.M., 2021. Exploring sources of variation in thermoluminescence emissions and anomalous fading in alkali feldspars. Radiat. Meas.141, 106541. https://doi.org/10.1016/j.radmeas.2021.106541.

Ritter, B., Stuart, F.M., Binnie, S.A., Gerdes, A., Wennrich, V., Dunai, T.J., 2018. Neogene fluvial landscape evolution in the hyperarid core of the Atacama Desert. Sci. Rep. 8, 13952. https://doi.org/10.1038/s41598-018-32339-9.

Ritter, B., Wennrich, V., Medialdea, A., Brill, D., King, G., Schneiderwind, S., Niemann, K., Fernández-Galego, E., Diederich, J., Rolf, C., Bao, R., Melles, M., Dunai, T.J., 2019. "Climatic fluctuations in the hyperarid core of the Atacama Desert during the past 215 ka". Sci. Rep. 9, 5270. https://doi.org/10.1038/s41598-019-41743-8.

Sager, C., Airo, A., Arens, F.L., Schulze-Makuch, D., 2021. New type of sand wedge polygons in the salt cemented soils of the hyper-arid Atacama Desert. Geomorphology 373, 107481. https://doi.org/10.1016/j.geomorph.2020.107481.

Schaetzl, R.J., Running, G., Larson, P., Rittenour, T., Yansa, C., Faulkner, D., 2021. Luminescence dating of sand wedges constrains the Late Wisconsin (MIS 2) permafrost interval in the upper Midwest, USA. Boreas. https://doi.org/10.1111/bor.12550.

Sellwood, E.L., Guralnik, B., Kook, M., Prasad, A.K., Sohbati, R., Hippe, K., Wallinga, J., Jain, M., 2019. Optical bleaching front in bedrock revealed by spatially-resolved infrared photoluminescence. Sci. Rep. 9, 2611. https://doi.org/10.1038/s41598-019-38815-0.

Smedley, R.K., Duller, G.A.T, Pearce, N.J.P, Roberts, H.M. 2012. Determining the K-content of single grains of feldspar for luminescence dating. Radiat. Meas. 47, 790–796. https://doi.org./10.1016/j.radmeas.2012.01.014.

Sontag-González, M., Li, B., O'Gorman, K., Sutikna, T., Jatmiko, Jacobs, Z., Roberts, R.G., 2021. Establishing a pIRIR procedure for De determination of composite mineral grains from volcanic terranes: A case study of sediments from Liang Bua, Indonesia. Quat. Geochronol. 65, 101181. https://doi.org/10.1016/j.quageo.2021.101181.

Stone, A., Bailey, R.M., 2012. The effect of single grain luminescence characteristics on single aliquot equivalent dose estimates. Quat. Geochronol. 11, 68–78. https://doi.org/10.1016/j.quageo.2012.03.014.

Thomsen, K.J., Kook, M., Murray, A.S., Jain, M., 2018. Resolving luminescence in spatial and compositional domains. Radiat. Meas. 120, 260–266. https://doi.org/10.1016/j.radmeas.2018.06.002.

Thomsen, K.J., Murray, A.S., Jain, M., Bøtter-Jensen, L., 2008. Laboratory fading rates of various luminescence signals from feldspar-rich sediment extracts. Radiat. Meas. 43, 1474–1486. https://doi.org./10.1016/j.radmeas.2008.06.002.

Veit, H., Preusser, F., Trauerstein, M., 2015. The Southern Westerlies in Central Chile during the two last glacial cycles as documented by coastal aeolian sand deposits and intercalating palaeosols. Catena 134, 30–40. https://doi.org/10.1016/j.catena.2014.11.002.

Wallinga, J., Murray, A., Wintle, A., 2000. The single-aliquot regenerative-dose (SAR) protocol applied to coarse-grain feldspar. Radiat. Meas. 32, 529–533. https://doi.org/10.1016/S1350-4487(00)00091-3.

Williams, G., 1986. Precambrian permafrost horizons as indicators of palaeoclimate. Precambrian Res. 32, 233–242. https://doi.org/10.1016/0301-9268(86)90008-2.

Wintle, A.G., Murray, A.S., 2006. A review of quartz ptically stimulated luminescence characteristics and their relevance in single-aliquot regeneration dating protocols. Radiat. Meas. 41 (4), 369–391. https://doi.org/10.1016/j.radmeas.2005.11.001

This is a postprint, which has been submitted for peer-review to Quaternary Geochronology and has been published in its final version as Zinelabedin et al., 2022. Testing the potential of using coarse-grain feldspars for post-IRIRSL dating of calcium sulphate-wedge growth in the Atacama Desert. Quaternary Geochronology 71, 101341.

Supplementary Material

Testing the potential of using coarse-grain feldspars for post-IR IRSL dating of calcium sulphate-wedge growth in the Atacama Desert

Aline Zinelabedin[1*], Svenja Riedesel[2], Tony Reimann[2], Benedikt Ritter[1], Tibor J. Dunai[1]

[1] Institute of Geology and Mineralogy, University of Cologne, Zülpicher Str. 49b, 50674 Cologne, Germany, *Corresponding author: aline.zinelabedin@uni-koeln.de
[2] Institute of Geography, University of Cologne, Zülpicher Str. 45, 50674 Cologne, Germany

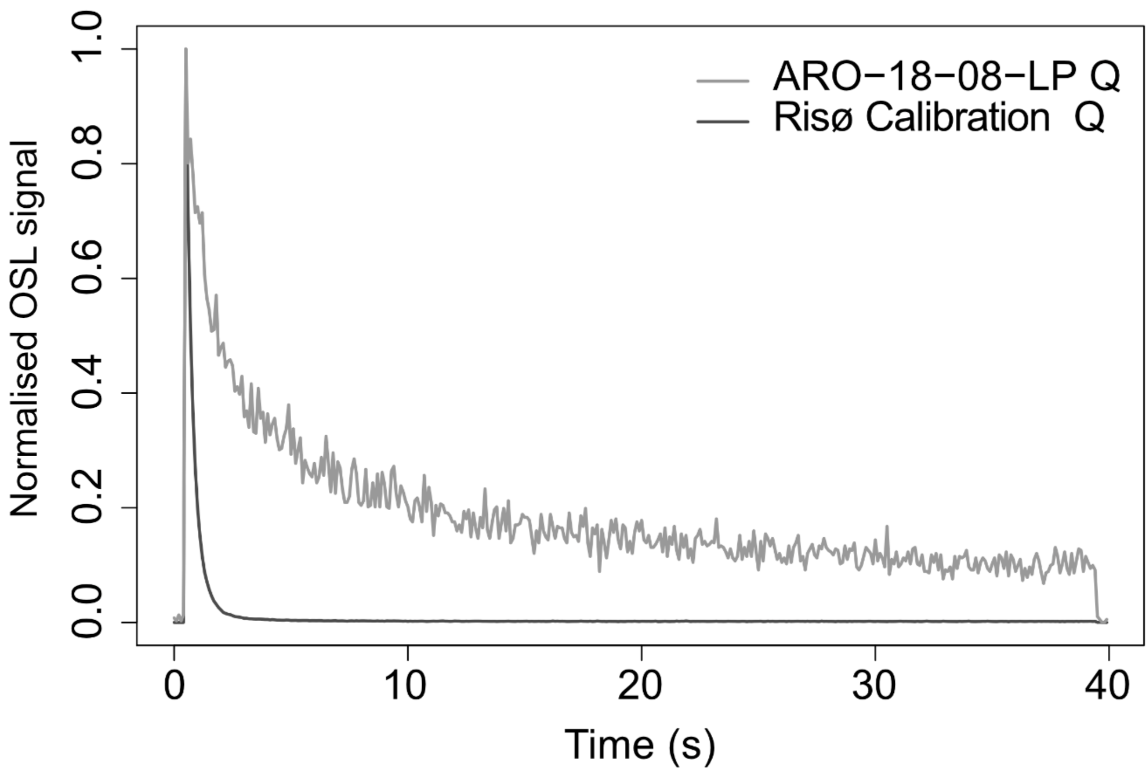

Fig.S1: Normalised OSL signal for coarse-grained quartz sample from ARO18-08-LP in comparison to a Risø calibration quartz. The OSL quartz signal of ARO18-08-LP is characterised by a dominant slow component and low OSL intensities.

This is a postprint, which has been submitted for peer-review to Quaternary Geochronology and has been published in its final version as Zinelabedin et al., 2022. Testing the potential of using coarse-grain feldspars for post-IRIRSL dating of calcium sulphate-wedge growth in the Atacama Desert. Quaternary Geochronology 71, 101341.

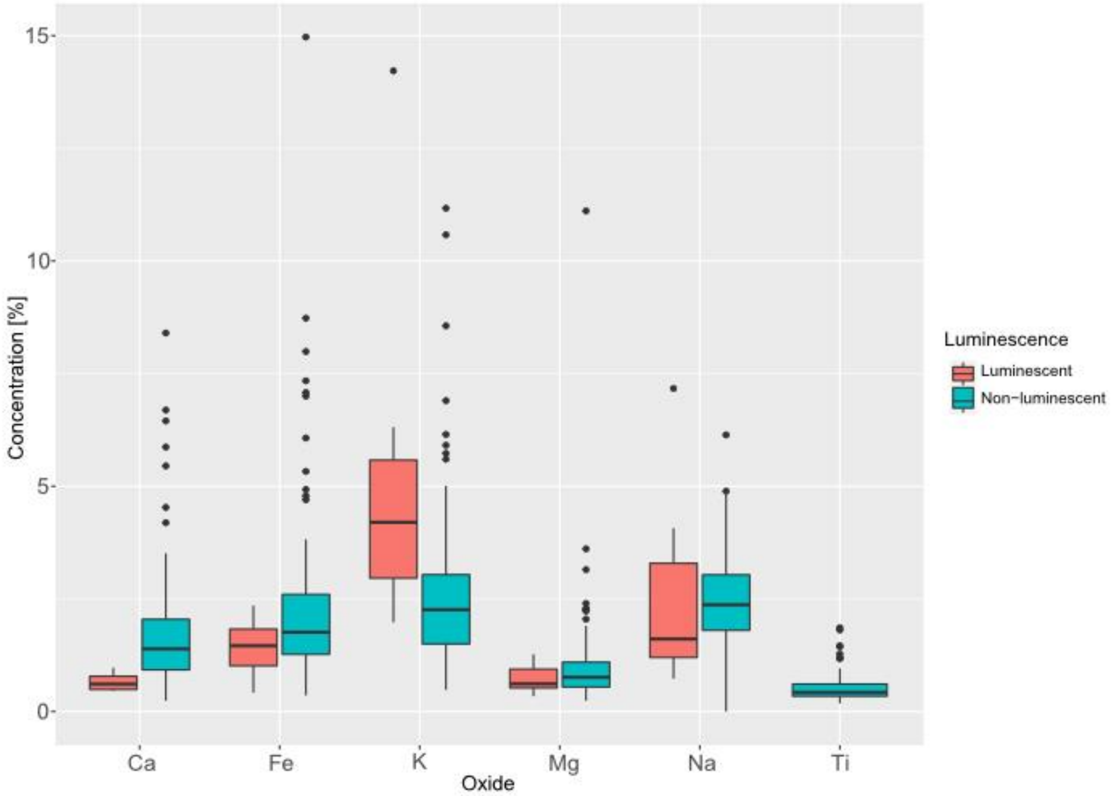

Fig. S2: Statistical distribution of all investigated oxide concentrations from feldspar grains of three single-grain discs of ARO18-08-LP including luminescent (red) and non-luminescent (turquoise) grains.

This is a postprint, which has been submitted for peer-review to Quaternary Geochronology and has been published in its final version as Zinelabedin et al., 2022. Testing the potential of using coarse-grain feldspars for post-IRIRSL dating of calcium sulphate-wedge growth in the Atacama Desert. Quaternary Geochronology 71, 101341.

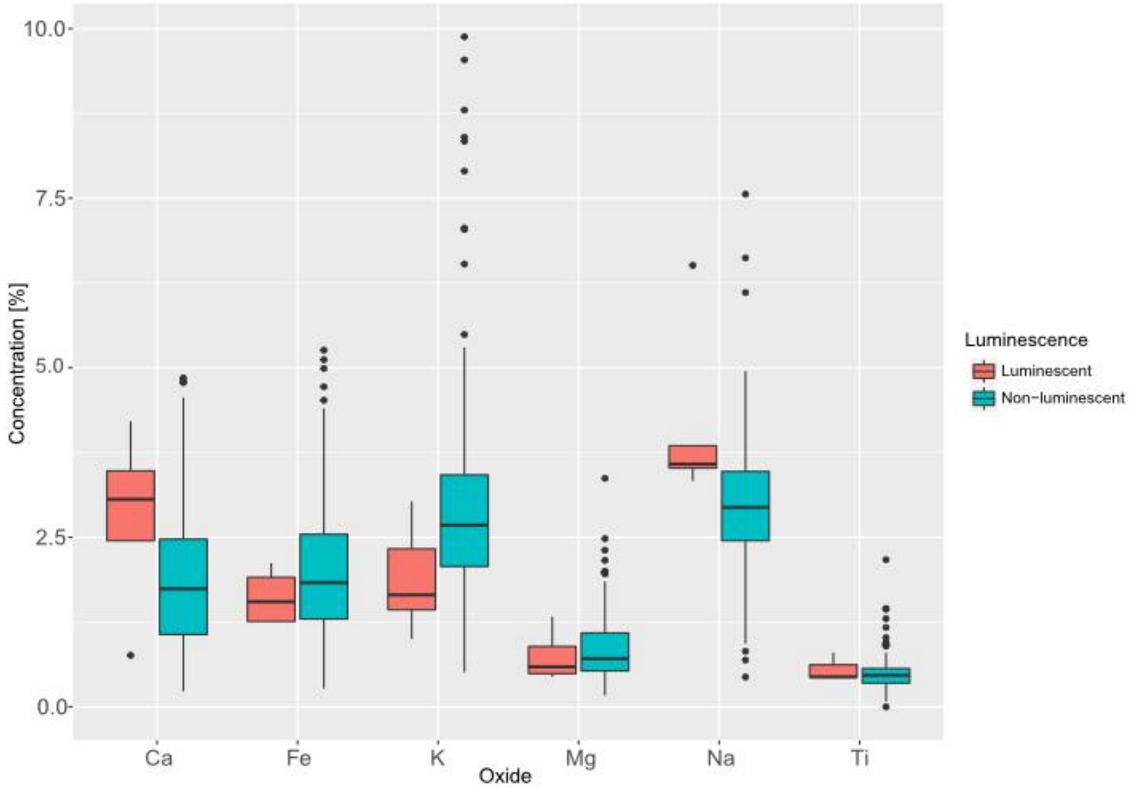

Fig. S3: Statistical distribution of all investigated oxide concentrations from feldspar grains of four single-grain discs of ARO18-08-RP including luminescent (red) and non-luminescent (turquoise) grains.

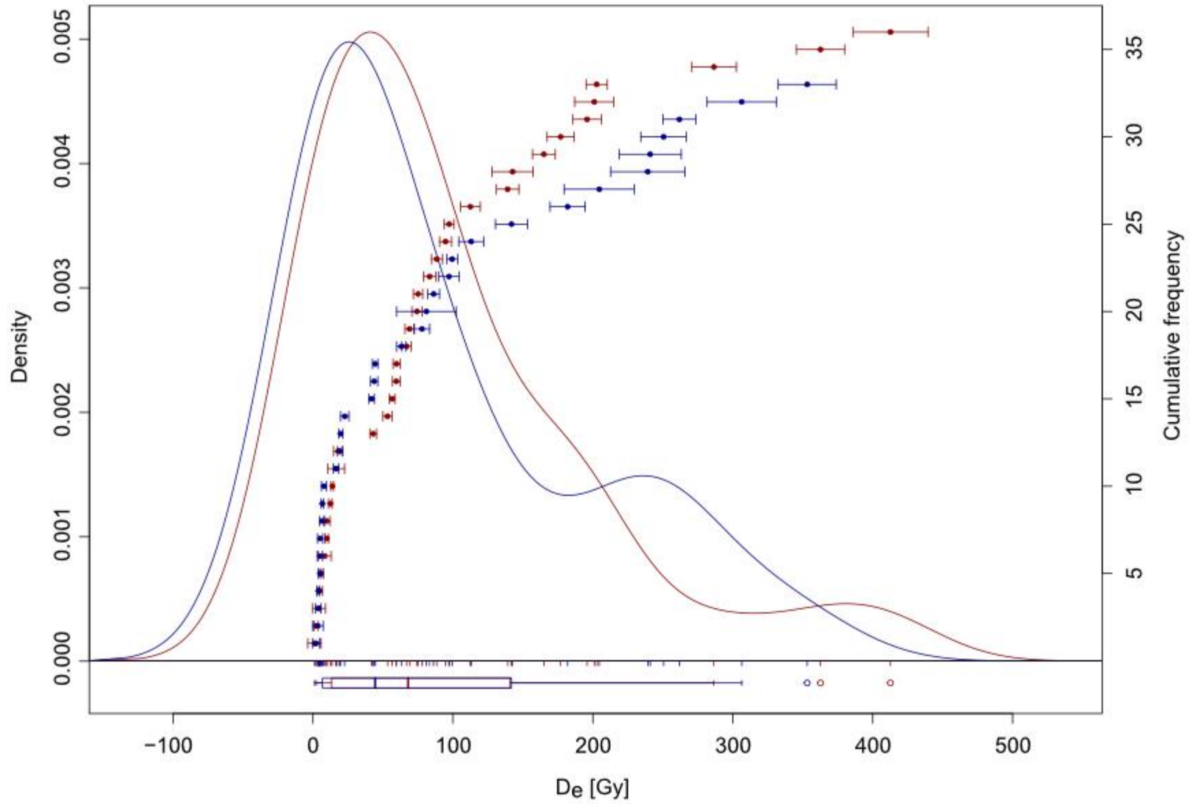

Fig. S4: $IRSL_{50}$ equivalent doses from 1 mm aliquots of two samples ARO18-08-LP (blue) and ARO18-08-RP (red). ARO18-08-LP: Total number of measured discs = 62, accepted = 33, saturated = 3, do not passed rejection criteria = 26. ARO18-08-RP: Total number of measured discs = 56, accepted = 36, saturated = 1, do not passed the rejection criteria = 19.